Sustainable Cities and Society 71 (2021) 102959

Contents lists available at ScienceDirect

Sustainable Cities and Society

journal homepage: www.elsevier.com/locate/scs

Designing and assessing solar energy neighborhoods from visual impact

Pietro Florio [a,*], Giuseppe Peronato [b], A.T.D. Perera [c], Anthony Di Blasi [b], Kin Ho Poon [d], Jérôme H. Kämpf [b]

[a] Solar Energy and Building Physics Laboratory LESO-PB, EPFL, Switzerland
[b] Idiap Research Institute, Martigny, Switzerland
[c] Urban Energy Systems Group, Swiss Federal Laboratories of Materials Science and Technology, EMPA, Switzerland
[d] Solar Energy Research Institute of Singapore (SERIS) & Department of Building, National University of Singapore (NUS), Singapore

ARTICLE INFO

Keywords:
Solar energy in cities
BIPV
Energy planning
Energy-hub
Visual impact
Load match

ABSTRACT

The optimal diffusion of Building Integrated PhotoVoltaics (BIPV) in cities requires diligent planning to arrange temporal and spatial distribution of energy, while preserving the aesthetics of city landscapes. Benefitting from an increasing quality of 3D models of cities, a comprehensive methodology to estimate potential energy generation from visually-acceptable PV, energy use from buildings, and economically viable micro-grid operation is proposed, by combining validated dynamic energy simulation tools into an open-source computational platform. The platform intends to be useful for urban planners and officials in charge of planning a large-scale BIPV installation into an existing neighborhood: simulations are carried out at the city scale, inclusive of façade potential, shading from vegetation and detailed roof shapes with super-structures.

Social acceptability is investigated through a novel visual impact assessment methodology and grid integration solutions are analyzed with reference to their associated costs. Under a conservative scenario, a median of 10 kW $h_{AC\text{-}electricity}$ / m^2 heated floor area per year is available from BIPV production in Geneva (Switzerland), covering 32 % electricity demand for space heating from heat pumps, or, alternatively, almost 10 times the one for space cooling. Visual impact has demonstrated not to be concurrent to grid integration constraints at the current stage, but rather to contribute to filtering building envelope surface and avoid grid curtailment of excess electricity. In the near future, with an increased grid efficiency, visual impact is expected to become a crucial criterion to limit the integration extent.

1. Introduction

EU member states are committed to reduce Green House Gas (GHG) emissions due to buildings by 60 %, their energy consumption by 14 %, and energy consumption of heating and cooling by 18 %, aiming at a 55 % reduction in emissions by 2030 (European Commission, 2020b), 50 % in Switzerland (Swiss Federal Council, 2019). Most of this share is imputable to pre-2000 constructions, which represent 85 % of the European building stock, despite being far from the end of their life cycle. As up to 95 % of such buildings is expected to remain operational until 2050 (European Commission, 2020b; Trovato et al., 2020), an improved energy efficiency strategy integrated with Renewable Energy Sources must be drafted in the short term.

Solar energy has a prominent role in guaranteeing a renewable and distributed energy supply to urban areas, especially by taking advantage of solar radiation reaching building surfaces. Buildings' envelope could potentially become an active surface by producing energy: solar power production potential, which could be issued from Building Integrated Photovoltaics (BIPV), could cover between 24 % and 40 % of the electricity demand in EU countries (Osseweijer et al., 2018) and above 40 % in Switzerland (Walch et al., 2020). It is foreseen that more than half of the global Photovoltaic (PV) capacity from 2015 to 2050 will be being installed on buildings, producing almost half of the total PV electricity targets (International Energy Agency IEA, 2014). This trend is also enhanced by the continuous reduction in the price of solar technologies (Jäger-Waldau et al., 2019), and by specific incitation programs (European Commission, 2020a; Swiss Federal Office of Energy, 2019), involving citizen communities.

In the light of the above reflections, a crucial dilemma comes to evidence: how to refurbish a gradually obsolescent building stock according to Green Economy criteria, in an economically viable manner, while preserving the identity of urban districts, especially their cultural

* Corresponding author.
E-mail address: pietroflorio@gmail.com (P. Florio).

https://doi.org/10.1016/j.scs.2021.102959
Received 21 December 2020; Received in revised form 1 April 2021; Accepted 21 April 2021
Available online 25 April 2021

heritage? Does a comprehensive planning method for the renovation of urban areas with the integration of solar technologies exist?

Nowadays, the possibility of adding (i.e., not integrating) PV modules on building façades or rooftops is often considered at the end of the design or renovation process, thus limiting the alternatives to visually unappealing solutions. Most solar modules in existing urban areas are positioned on roofs, where the prevalent amount of solar radiation is available and less invasive scaffolding is needed for installation. Building-attached systems, i.e., roof-added systems, are easy to install, maintain, and remove, making them preferred by end-users and energy contracting companies in case of controversies. For example, the Swiss legislation only grants waivers of building permit for solar systems on rooftops (Giuseppe Peronato, 2019).

Kosorić et al. (2018) define a steering framework for PV integration into existing residential buildings in Singapore. Such multi-criteria decision-making (MCDM) method covers electricity generation performance as well as economic, environmental, spatial/urban, functional, aesthetic and social aspects at different stages of the PV integration process. MCDM is useful for balancing the various conflicting criteria that determine certain system parameters. Azzopardi et al. (2013) and Thebault et al. (2020) propose an ELECTRE III-based MCDM method aiming at the selection of suitable PV technologies, given the technical, environmental and economic context, adapted for urban-scale applications.

Current solar maps focus on solar irradiation availability as the main criterion for sorting the suitability of sun-exposed building surfaces (IRENA, 2019; Kanters et al., 2014; Lobaccaro et al., 2019), which is often combined with a suitability assessment of surfaces based on a given irradiation threshold (Kanters et al., 2014). Previous research has also included other criteria, such as, for example, a match with the energy consumption (Costanzo et al., 2018; Groppi et al., 2018) also to minimize storage needs (Freitas et al., 2018), an economic ranking based on payback time (Jakubiec & Reinhart, 2013; Lee et al., 2018; Mansouri Kouhestani et al., 2019), geometric regularity of PV module arrangement (Peronato et al., 2015), structural (Thebault et al., 2020) and heritage suitability (De Medici, 2021; Lucchi et al., 2014; Thebault et al., 2020). Downscaling to hourly generation potential on rooftops has been even achieved at country level (Walch et al., 2020). Even if most studies and available solar cadasters are limited to roofs, the solar potential of façades has been investigated based on extended 2.5D calculation methods (Catita et al., 2014), fully 3D simulations (Peronato et al., 2016), and refined potential based on typological analysis and simulations at higher Level of Detail (Saretta, 2020). The influence of vegetation has also been considered in previous works (Lukač et al., 2013), also with respect to its modeling uncertainty (Peronato, Rastogi et al., 2018; Peronato, Rey et al., 2018).

Certainly, the adoption of BIPV on vertical facades is becoming more popular. However, more architectural integration issues and legal constraints must be considered during the design phase. Widely customized BIPV are required on vertical facades, especially for heritage buildings, where high visual impact or reflection glare may become a particular concern (Munari Probst & Roecker, 2019; Lingfors et al., 2019). Even if results may be country-dependent, a survey showed how roof PV integration designs have a higher aesthetic score than the roof and facade ones in general (Kosorić et al., 2018): this means that the high visibility of façades is a crucial variable, independently from the quality of the employed products and the integration finish (Florio, 2018). Rare scientific literature is available on the visibility extent of solar modules in urban contexts but practitioners assume 500 m for small scenic components (Cassatella, 2014, p. 36; Van der Ham & Idding, 1971), with explicit reference to building-integrated solar modules in Switzerland (Munari Probst & Roecker, 2019; Rezakhanlou & Frei, 2011, p. 9; Florio et al., 2017).

Beyond visual impact issues, the limitations in the local grid might notably reduce the integration of solar PV systems. Being a critical infrastructure, fluctuations brought by the local installation of PV panels can lead to cascade failures in the grid (Wang & Perera, 2020). The support of local storage, demand response strategies, etc. is vital in supporting PV integration besides simply calculating the power generation from each PV panel.

When analyzing the present state of the art, it emerges that existing methodologies are far away from the existing requirement where it is essential to: (i) evaluate the available PV potential at the building scale, inclusive of complex urban geometries, at a sufficient time resolution to consider daily dynamics; (ii) understand the visual impact and social acceptability, (iii) estimate the capability to accommodate PV into local energy infrastructure considering the local energy demand and the energy storage capacity at the microgrid level.

Conducting such a broad assessment is essential to enable large-scale deployment of PV panels at the urban scale. The present study addressed this research gap by introducing a novel design workflow to assess the potential of PV deployment at the urban scale accommodating public acceptance and the technical limitations of the grid, which will play a vital role in the energy transition, together with the economic feasibility. The model includes estimating potential PV generation on roofs and façades at hourly resolution, based on three-dimensional vector data, whose use is rapidly increasing due to the increasing diffusion of vector 3D city models (Biljecki et al., 2015). In spite of involving a quite expensive and complex process, 3D city models at high Level of Detal (LOD) are now also produced at the national or regional level (e.g., in Switzerland and the Netherlands) and can be then easily obtained through digital elevation models (Ledoux et al., 2021), which are available open-source for EU capital cities (*Building Height 2012 — Copernicus Land Monitoring Service, 2020*Building Height —Copernicus Land Monitoring Service, 2020*Building Height 2012 — Copernicus Land Monitoring Service, 2020*; *EU-DEM v1.1 — Copernicus Land Monitoring Service, 2020*), or through deep-learning techniques from Very High Resolution - VHR satellite imagery (Bischke et al., 2018). The building energy consumption and size of energy systems of a given district are computed as well at an hourly time step, by taking shading from vegetation and detailed roofing elements into account. The simulated electricity generation is used to select viable building envelope areas to install PV modules, with the filtering of visual impact to further refine the available PV area. The generated electricity is integrated into a district energy-hub, which dynamically adjusts the supply energy mix to minimize its cost and its impact on the infrastructure. The methodology is tested on a district in the urban area of Geneva, Switzerland.

2. Methodology

This research investigates three criteria to drive PV integration design and the associated energy-hub operation planning. The multi-criteria assessment includes:

1) Solar energy potential
2) Building energy consumption
3) Visual impact
4) E-Hub operation planning and optimization

These four elements build up a comprehensive neighborhood BIPV design methodology. Points 1), 2) and 4) are dynamically calculated for each hour of the weather file. The advantage of this workflow resides in the accurate match of demand and supply, which is totally simulation-based and does not rely on any specific input data apart from the district geometry (Level of Detail LOD2) and some indications on the buildings' use. As such, it is easily replicable and does not require thorough on-site supervision. Based on vector geometry, the proposed methodology includes façade energy generation potential and the results database can be easily queried and modified without having to deal with large raster datasets.

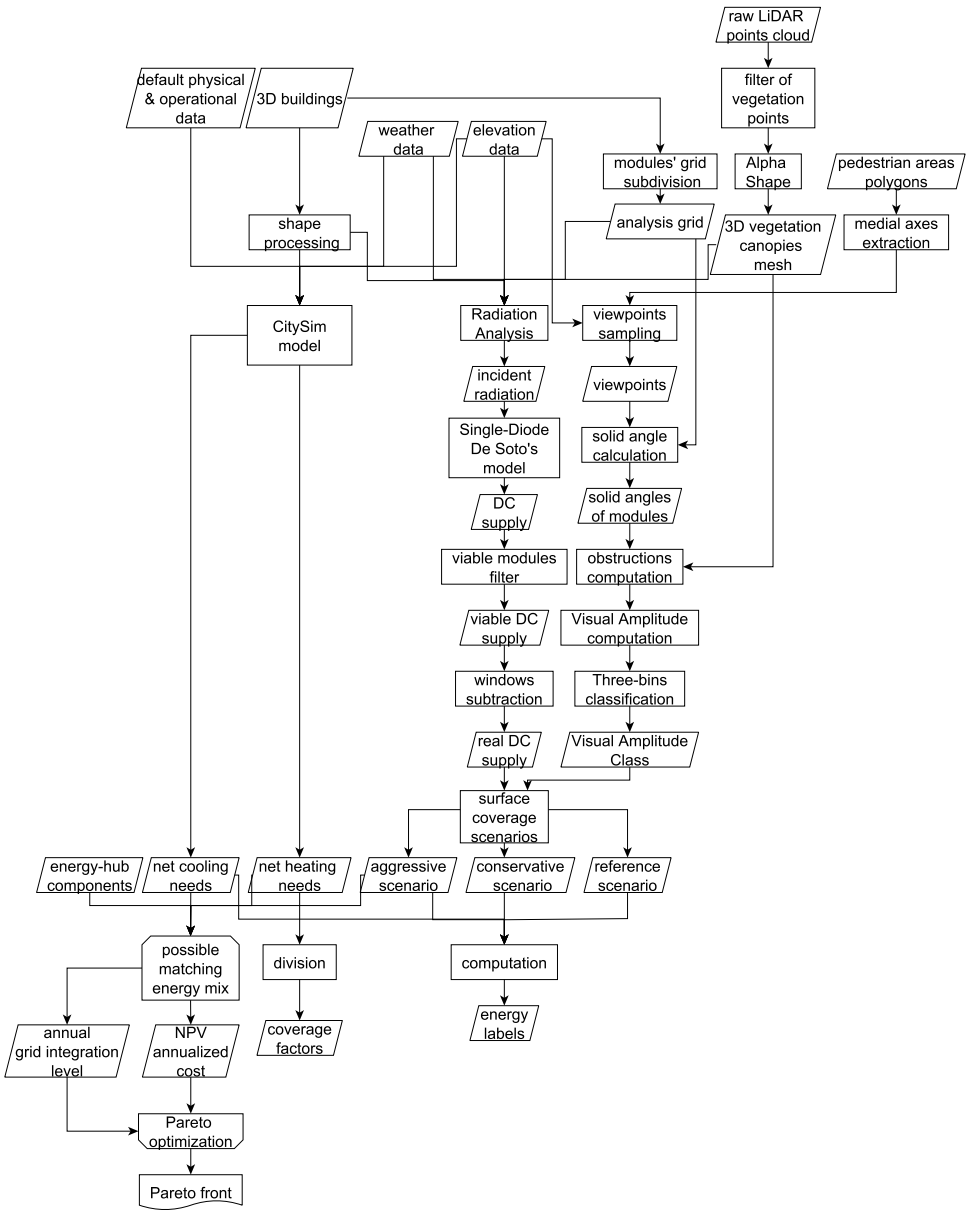

Fig. 1. Methodology flow-chart.

2.1. Study area

The applied computational tool is used in a large and diversified district in Geneva, Switzerland, an ideal place for such case studies due to its open geodata database. The selected district lies in the district of Eaux-Vives, a transformation area of the city which includes several different building typologies and uses. The district's 3D vector model was retrieved from the online open data repository of the Service d'Information du Territoire de Genève (SITG) (*SITG - Le Territoire Genevois à La Carte*, 2020). Over an area of 750 × 750 m with a buffer of 50 m for context buildings, a total number of 473 buildings was analyzed in terms of solar energy potential, visual impact and energy consumption (Fig. 1). To reduce the complexity in the computation, the study area was split in 9 tiles of 300 × 300 m with 100 m overlap bands: as such, mutual shadings from buildings are always accounted. The 3D model employed for all calculations is a LOD2 model, i.e., featuring accurate roof shapes, but also most of the overhangs and roof superstructures: even if it is still rare to find such detailed models, their availability is increasing. From the raw LiDAR point cloud, it was possible to extract the points relative to vegetation and cluster them together in triangulated meshes through a dedicated alpha-shape algorithm (Peronato et al., 2016).

2.2. Assessment of solar energy potential

Solar energy potential is assessed based on previously available studies (Peronato, 2019; Peronato, Rastogi et al., 2018; Peronato, Rey et al., 2018). The irradiance simulation relies on Daysim (Reinhart & Herkel, 2000), based on the backward raytracer RADIANCE: it simulates the hourly irradiance received on a building envelope surface within the study area including direct, diffuse and reflected irradiance. Daysim adopts a daylight coefficient approach that helps reduce computational time. Hourly irradiance simulation results generated by Daysim are processed by the PVLIB toolbox in Python to estimate the DC power generation of the installed PV modules. The De Soto five-parameter model (ideality factor parameter at SRC (eV), diode reverse saturation current at SRC (A), light current at SRC (A), series resistance at SRC (Ω) and shunt resistance at SRC (Ω) was used to retrieve the necessary input for the SingleDiode model (see Table 3) as implemented in the PVLIB

Table 1
Simulation settings of this study.

Items	Settings
Tool (Simulation engine)	Daysim (RADIANCE)
Grid size (test points distribution)	*Grid1* - 2 m *Grid2* – Depends on the size of the PV module
Reflective properties (reflectance)	Ground – 10 % Façade – 30 % Roofs – 20 % Vegetation – 20 %
Max no. of inter-reflections	2
Weather file	**Geneva** (Source: IWEC)
Sky density setting	Tregenza sky subdivisions (145 sky patches)

Table 2
Parameters of the alphaShape.

Radius (m)	Hole Threshold (m^3)	Region Threshold (m^3)
1.5	10	5

Table 3
Characteristics of the commercial 185 Wp PV model adopted in this work. Source: Peronato (2019).

Parameter			Source
Current at maximum power point [A]	I_{mp}	8.5	Manufacturer
Voltage at maximum power point [V]	V_{mp}	21.8	Manufacturer
Current at short circuit [A]	I_{sc}	9	Manufacturer
Open-circuit voltage [V]	V_{oc}	26.3	Manufacturer
Short-circuit current temperature coefficient [%/°C]	α_{sc}	+0.046	Manufacturer
Parameters for the De Soto model			**Source**
Product of the usual diode ideality factor [-], number of cells in series [-], and thermal voltage [V]	*a*	1.2	SUPSI
Photocurrent [A]	I_L	9	SUPSI
Diode reverse saturation current [A]	I_o	1.02e–10	SUPSI
Series resistance [Ω]	R_s	0.18	SUPSI
Shunt resistance [Ω]	R_{sh}	2200	SUPSI
Short-circuit current temperature coefficient [A/C]	$alpha_{sc}$	0.00414	$\alpha_{sc}/100 \cdot I_{sc}$
Energy bandgap [eV]	*EgRef*	1.121	Reference from (Dobos, 2012)
Temperature dependence of the energy bandgap [1/K]	*dEgdT*	−0.0002677	Reference from (Dobos, 2012)

toolbox. Unlike an approach based on a fixed efficiency at Standard Test Conditions (cell temperature of 25 °C, irradiance of 1000 W/m^2 and an air mass 1.5), these models consider the effect of the cell temperature and irradiance on the efficiency of the PV module, which is hence varying based on the supposed installation conditions. In particular, we assume here the most conservative conditions related to module temperature (i.e., with an insulated back), which are applied both on façade- and roof-integrated installations. The main advantage of the De Soto's model is that it relies on a few parameters that are generally available from the manufacturer. A commercial monocrystalline BIPV model is selected as the type of PV module in this study (Table 3), adopted in all buildings for simplicity. This particular model was chosen as available at the time in the Swiss market and adopted in high-end BIPV installations.

Simulation settings (Table 1) include the 1) arrangement of sensor points; 2) settings of buildings, terrain & vegetation; 3) and weather input. Concerning the arrangement of sensor points, they are placed at the nodes of two different grids.

- *Grid1* is applied on building surfaces, both roofs and façades, and is defined as a 2-m structured grid, i.e., a fixed-spacing grid, with nodes at a 2-m distance. On envelope surfaces that are too small to fit a 2-x-2 m square, a sensor point is placed at the center. The 2-m resolution is considered appropriate by previous studies (Peronato, Rey et al., 2018).
- *Grid2* is designed to represent the sensor points placed on PV modules. It is a structured grid characterized by a fixed spacing that corresponds to the size of a given PV module. In this work, a commercial module available in Switzerland with a 1.30 × 0.88 m size is used, Only surfaces fitting at least one module are considered. These surfaces are only retained in a first step and further refined when checking for geometry and viability criteria (see further on in this section).

The simulation of solar irradiances is conducted on *grid1*. Results are then remapped to the denser *grid2*. The value of each node is interpolated from *grid1* to *grid2* using an Inverse Distance Weighting (IDW) algorithm, which is based on the Euclidean distance in the x, y planes of each *grid2* point from the 3 closest points on *grid1* having the same normal.

This approach based on two structured grids has two advantages: reducing the simulation time, by conducting the simulation on a coarser grid, while selecting only the surfaces that can actually fit the PV modules.

Regarding vegetation, the mesh of tree canopies is generated by the MATLAB function *alphaShape* from filtered airborne laser scanned (LiDAR) point clouds. The AlphaShape parameters are presented in Table 2. The MATLAB script is available in this repository (Peronato, 2018).

The DTM raster grid representing the terrain is transformed into a mesh using the "MeshPatch" function in Rhino. The resulting triangular mesh is simplified by a "ReduceMesh" function to reduce the number of faces and hence the simulation time. These operations are carried out in the Rhino-Grasshopper 3D modelling environment (Robert McNeel & Associates, n.d.).

The weather data for Geneva is issued from a typical weather file (IWEC) obtained from the EnergyPlus repository. This study adopts the specifications of a commercial solar roof system as the PV simulation input. It consists of a 185 Wp module with an energy conversion efficiency of 17.3 %. The size of each module is 1300*875*6.5 mm. The characteristics of this system are listed in Table 3 (Peronato, 2019).

To make the installation scenarios more realistic, some viability constraints are adopted: i) a minimum of four adjacent panels is required on roofs to install the PV modules, two on facades; such amount is intended to avoid a visually unpleasant patchwork effect on building envelopes, even if is some cases it might be beneficial (Freitas et al., 2015). ii) A gap is inserted every two modules on façades, to simulate the presence of windows; iii) a minimum of 120 kW h_{AC} / year, considering an average inverter efficiency of 85 % (conservative value), is required per module, otherwise it is discarded.

2.3. Building energy consumption assessment

The building energy consumption assessment relies on CitySim (Robinson et al., 2011), an urban energy simulator modeling energy and matter fluxes at the urban scale in a reasonable computing time frame by using simplified physical models. The developed solver is based on the Simplified Radiosity Algorithm (Robinson & Stone, 2004) for the outdoor illumination, a split-flux method for the indoor illumination (Robinson & Stone, 2006), and a simplified resistor-capacitor model for dynamic thermal behavior indoors (Kämpf & Robinson, 2007). Validation of the simplified thermal model in comparison with other Building Energy Models (BEM) was carried out using the BESTEST (Walter & Kämpf, 2015). The building occupants' presence and behavior are modeled through deterministic schedules like in any Buiding Energy Model, but also using stochastic models (Haldi & Robinson, 2011).

The CitySim Database Linker, introduced in a former study (Mohajeri

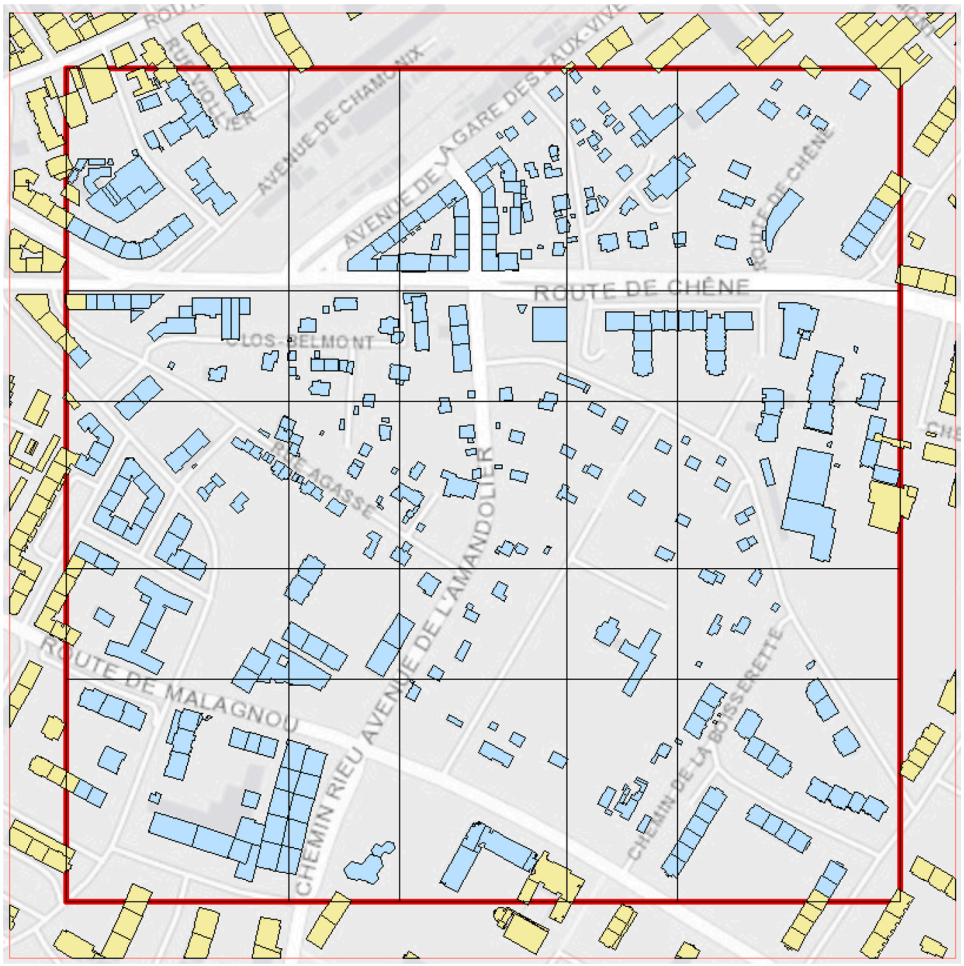

Fig. 2. Study area in the district of Eaux-Vives, Geneva (Switzerland). In blue the analyzed buildings, in yellow the context buildings within the buffer zone.

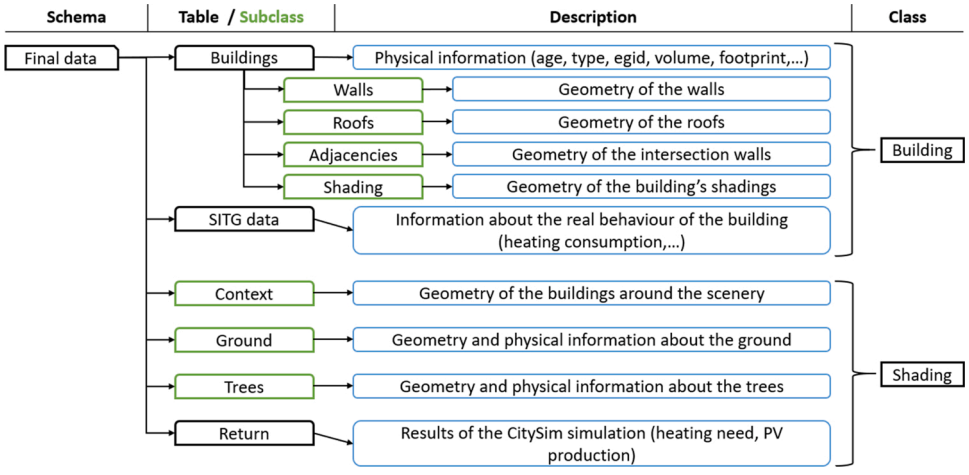

Fig. 3. The database schema structure Final_data containing the main information relating to the case-study.

et al., 2016) as a Java program to link information in a dedicated PostgreSQL database with the CitySim Solver was used. The information relating to the case-study was gathered and inserted into the database with a specific structure. Such structure is based on two main schemas: *Final_data* contains neighborhood's information regarding buildings, terrain and trees (see Fig. 2), including all geometries, while *Default_data* (shown in Fig. 3) contains basic physical and operational information of the buildings, necessary to run the CitySim solver (the composition of different envelope types, occupancy and electric devices usage profile per type of building).

The *Final data* scheme is subdivided in two main classes of objects: building and shading (Fig. 2 on the right). The *building* class of objects describes the analyzed building components in the scene and their energy indexes. The *shading* class of objects contains features that mainly influence the incoming solar radiation, such as trees and adjacent buildings (i.e., context geometry).

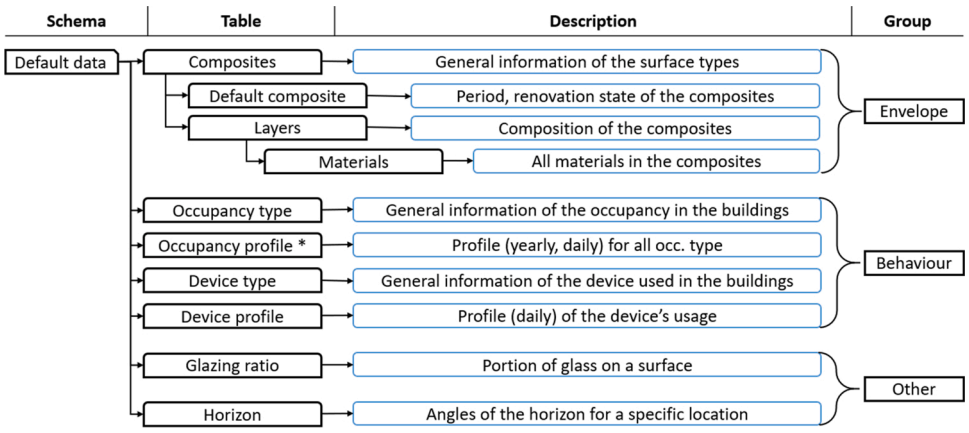

Fig. 4. The database schema structure Default_data containing the default physical and occupational characteristics of the buildings for the case-study.

Table 4
Default physical characteristics of the buildings with missing identifier (EGID).

Name	Value	Unit
Floor's height	2.4	m
Construction year	1900	–
Building type	Other	–
Renovation	no renovation	–

The *Default_data* scheme (in Fig. 3) contains the default physical and occupational characteristics of the buildings. The construction composites of walls, roofs and floors, together with all the information regarding the presence of occupants and their activities are matched with a typological collection based on building type and age. Further details, such as the glazing ratios, windows' U-values and g-values are also linked with the construction period. Detailed information regarding the assumptions can be found in (Perez, 2014).

All data imported in the database was provided by the Canton of Geneva through its official public repository (*SITG - Le Territoire Genevois à La Carte*, 2020). The main physical information regarding the building stock, i.e. age, use category, heated volume, etc. is also issued from the Geneva State geoportal. The 3D geometry of the buildings was processed in Rhino-Grasshopper (Robert McNeel & Associates, n.d.) to match the requirements of the simulation software: the orientation of the surfaces (the normal should point outwards), the number of surfaces (merging adjacent surfaces with the same normal), the deletion of the contiguous walls (i.e., shared between two buildings). The geometry was imported in PostGIS via QGIS (QGIS Development Team, n.d.) to fit in the database. The same method was applied to the terrain and the context geometry. The vegetation mesh created for the solar simulation was converted to a set of canopies' slices (planar surfaces), as illustrated in Fig. 4, to fit the CitySim's tree model, while reducing the complexity of complex 3D meshes. It should be noted that algorithm processing the geometry was automated and generalized to enhance the replicability of the method, even though some manual modifications had to be carried out in order to guarantee a better accuracy of the simulation.

A unique identifier of all buildings in Switzerland was used as the primary key in the database to join physical information. Unfortunately, the join was not always successful due to missing data. In such cases, the corresponding building geometry was associated with default values, as indicated in Table 4.

2.4. Visual impact assessment

In this paper, a first quantification of the visual stimulus based on solid angles is proposed (Florio et al., 2016, 2018). Visual targets, such as building envelopes that could host solar modules, are decomposed in triangular meshes in Rhino. A set of viewpoints is sampled on the medial axis of pedestrian areas and sidewalks, with a given spacing distance (2.5 m) (Fig. 5). The solid angle Ω [sr] that mesh facets subtend from

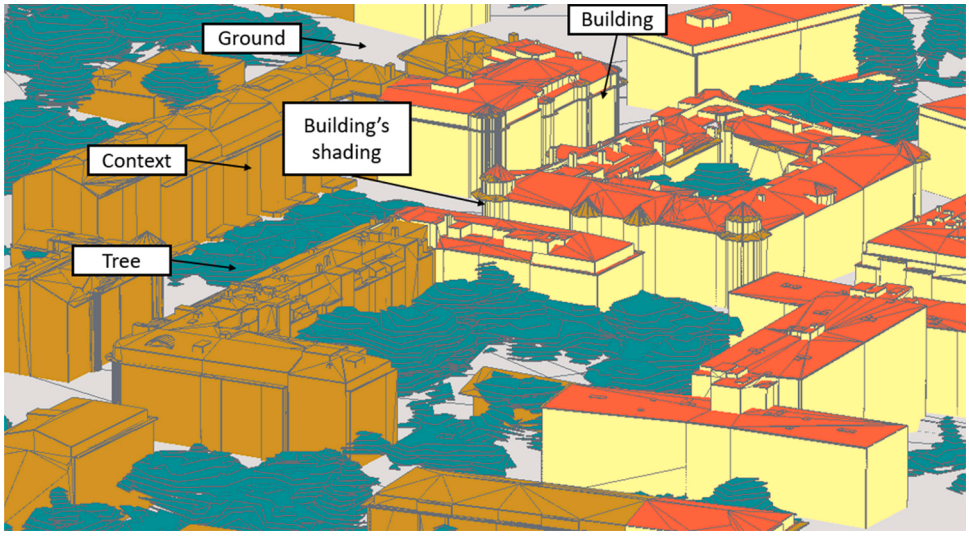

Fig. 5. 3D visualization of buildings, grounds and trees in the graphical user interface of CitySim.

each viewpoint is computed through the Van Oosterom's equation (Van Oosterom & Strackee, 1983) in the Grasshopper parametric module for Rhino (*Grasshopper 3D, Algorithmic Modeling for Rhino*, n.d.): a dedicated Python script has been set up by the authors to simplify this operation (Florio, 2019/2019). This value is weighted by the illuminance induced on mesh facets from isotropic light sources placed at the viewpoints' locations with visual obstruction E_w [lx], against the illuminance without visual obstructions E [lx]: visual obstructions, such as vegetation and other context elements, project shading on building envelopes, thus affecting the illuminance and the weighted solid angle Ω_w [sr] accordingly. Tree canopies are included in the model with a canopy permeability to 'visibility rays' *tcp* of 50 % (Eq. (1)), for other objects *tcp* is equal to 100 %.

Subsequently, the average solid angle Ω_m [sr] subtended by all viewpoints on each single triangular mesh facet is calculated to interpolate the mean perception of pedestrians in the district. The outcome is divided by the smallest perceptible stimulus for a human eye Ω_0 [sr] (i.e., the threshold), equivalent to one square minute of arc for high luminance contrast conditions (Shang & Bishop, 2000). The resulting variable is named "visual amplitude" VA [LogMAR] (Eq. (2)), as it represents the perceived size of the target mesh facet over the spherical field of view of the average observer (Fig. 6).

$$\Omega_w = \Omega \cdot \frac{E_w}{E} \cdot tcp \tag{1}$$

Eq. 1 Weighted solid angle

$$VA = Log_{10}\sqrt{\frac{\Omega_m}{\Omega_0}} \tag{2}$$

Eq. 2 Visual amplitude

The visual amplitude of a feature can be measured on an optometric scale, representing the size of the feature as perceived from a standard observer with no visual deficit in terms of visual acuity. Both visual acuity and visual amplitude are quantified using the base 10 logarithm of the Minimum Angle of Resolution (MAR), designated by LogMAR. For planar surfaces, the visual amplitude domain at 1 min of angle observer's visual acuity threshold ranges from minus infinity, in case of an infinitesimal surface, to 3.94 LogMAR, in case the observer lies on the surface plane subtending a solid angle of 2π steradians. If the surface subtends a solid angle equal to the threshold of 1 min squared, visual amplitude returns 0 LogMAR.

For the sake of this work, the visual impact of each point in the *grid2* set has been categorized into three increasing bins: low visibility, below 0 LogMAR, i.e., the perceptual threshold for the standard observer; medium visibility, between 0 and 1.4 LogMAR, as it could be easily perceived by most observers without particular visual impairment; high visibility, above 1.4 LogMAR, which means the target is clearly visible by all pedestrians. Visual impact represents a concern in Switzerland, where local population demonstrates a special affection for landscape and can raise opposition by the municipal authority to the installation of solar modules. An objective quantification of visual impact may represent a decision criterion for the authority to proceed with the enquiry.

2.5. Energy system planning

The previous sections presented the methodology developed to evaluate the available solar energy potential on building roofs and facades while reducing the visual impact. It is important to investigate how far we can accommodate the solar energy potential available on buildings' envelopes into the energy system. To identify the technical feasibility from the energy system perspective, it is essential to point out the limitations of energy conversion, grid curtailments, etc. The option adopted in this paper is to use a detailed energy system design tool, which provides a more comprehensive overview of the technical feasibility to integrate solar PV technologies into the buildings. Towards this objective, the energy hub model introduced by Geidl et al. (2007) is used in this study. A multi-energy hub consisting of solar PV panels, battery storage, heat pumps, and a dispatchable energy source (CHP), which caters to the local electricity and heating demand, is considered in the study. The multi-energy hub is expected to be interacting with the local electricity grid within grid curtailments for injecting and purchasing electricity. The optimal capacities for these components are derived using a bilevel optimization algorithm tool introduced by Perera et al. (2017a, 2017c). A comprehensive explanation about the energy model, optimization algorithm and the parameter values for the model are explained in Perera et al. (2017a, 2017c). The design tool evaluates the technical limitations for solar PV integration. A Pareto optimization is conducted considering the Net Present Value (NPV) of the system and the Grid Integration level (GI) as objective functions. Power supply reliability is considered as a constraint in the optimization.

Lower GI indicates a higher autonomy level that supports large penetration of the solar PV integration. However, limitations for grid integration imposed during the energy system optimization (grid curtailments) will make it mandatory to have reasonable energy storage and avoid reducing the renewable energy generated. This can often lead to an increase in the energy system's cost, creating a Pareto front between GI and cost. Therefore, it is important to consider the optimal system designs obtained, considering GI and NPV when evaluating the technical limitations for PV integration. Grid integration levels can be defined in several ways. The present study is using the formulation introduced by Perera et al., according to Eq. (3) (Perera et al., 2017b).

$$GI = \left(\sum_{\forall t \in T} P_t^{IG}\right) \Big/ \sum_{\forall t \in T} \left(P_t^{D,E} + \phi P_t^{D}, H\right) \tag{3}$$

Eq. 3 Grid Integration

$$NPV = ICC + \sum_{\forall d \in D}\left(OM_d^{Fixed} CRF_d + \sum_{\forall h \in H} PRI^{l} OM_{d,h}^{variable}\right), \forall t \in T, \forall d \in D, \forall h \in H \tag{4}$$

Eq. 4 Net Present Value

In this equation, P_t^{IG} and P_t^{D} denote the amount of energy imported from the grid and the energy demand, respectively, including both heat and electricity, at a time step t ($\forall t \in T$). ϕ denotes the heat to electricity ratio assumed as 0.33.

The NPV of the system consists of initial capital cost (ICC) and operation and maintenance cost (OM). ICC covers the acquisition and installation cost of the system components. Similarly, Operation and maintenance cost consists of fixed ($OM_{c,x}^{Fixed}$) and variable ($OM_c^{variable}$) components. NPV is formulated according to Eq. (4).

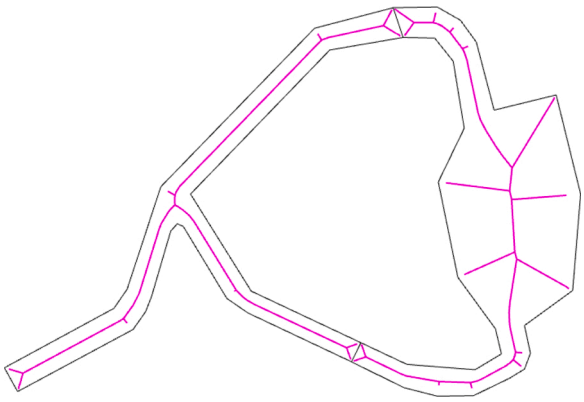

Fig. 6. Example of medial axis extraction of a fictional road or sidewalk segment (plan view), made of two polygonal shapes.

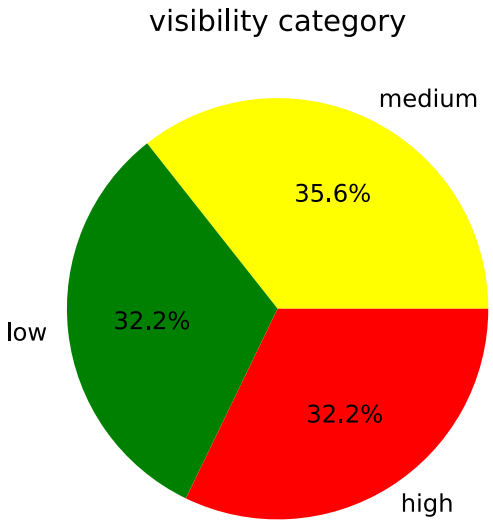

Fig. 7. Distribution of the buildings' envelope surface in the three visibility categories.

In the same equation, CRF_d denotes the Capital Recovery Factor for the c^{th} component. PRI indicates the real interest rate calculated using interest rates for investment and the local market annual inflation ratio. The cost values used in this study are based on previous work conducted specifically for Geneva (Siraganyan et al., 2019).The considered year is represented by h. A bi-level dispatch strategy is used to present the operation of the energy system. Evolutionary algorithm is used to support the optimization process, which is explained in detail in Perera et al. (2020).

3. Results

The overall assessment of PV generation potential and its limitations due to the visual impact and the grid limitations highlight the potential of PV technologies at the district scale. Towards this objective, the first part of this section presents the visual impact of building surfaces that could accommodate BIPV, and several consequent scenarios of PV electricity supply. However, integrating BIPV into the local grid depends on the fluctuations of PV generation and the building stock's energy demand. Accurately assessing the energy demand plays a vital role in this regard, as it helps quantify solar PV integration, here presented in the second part. The final part is devoted to quantifying the PV integration considering the grid curtailments and the energy storage limitation.

From the visual impact analysis, the envelope surface available in the analyzed district is almost equally distributed among the three categories (low, medium and high visibility) (Fig. 7): obviously, most façades lie in the high visibility category, some in medium, while most roof pitches lie in the low visibility category, some in medium (especially pitched roofs). Based on the visibility category, two scenarios of

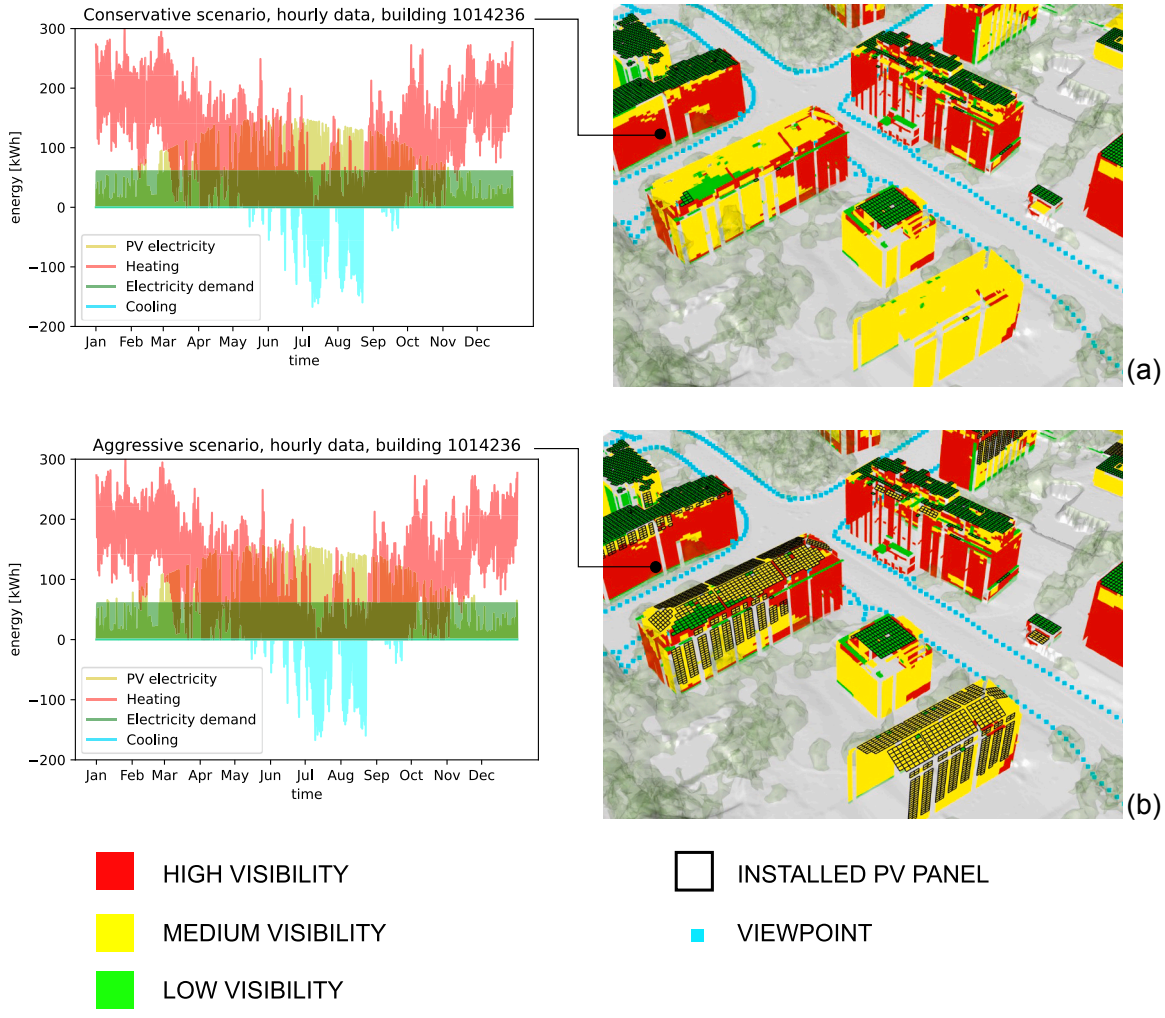

Fig. 8. Scenarios of BIPV installation based on visual impact categories: (a) conservative scenario and (b) aggressive scenario.

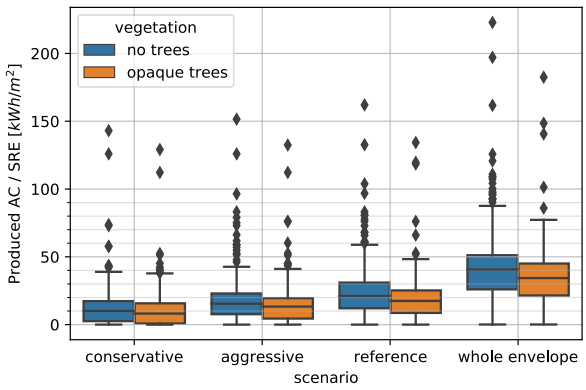

Fig. 9. Specific AC production issued from PV modules, according to the scenario and the presence or absence of vegetation in the 3D model.

BIPV distribution on building envelopes have been simulated: a conservative scenario, for which only *grid2* points in low visibility range are selected to host a PV module (Fig. 8a); an aggressive scenario, for which also medium visibility points are included (Fig. 8b). Such scenarios may seem unrealistic when envisioning large portions of the envelope covered in polished, shiny blue crystalline silicon cells: however, high integration standards may lead to colored, even textured protective glasses laminated on the modules, which could change their appearance completely at the cost of a lower conversion efficiency. The purpose of this work is to provide an overall estimation of the PV potential, without going into considerations of building-specific integration strategies.

The specific PV production per square meter of the Heated Floor Area was calculated for 304 buildings that have the surface information available on the database, considering an average inverter efficiency of 85 % (conservative value). Compared to the reference scenario, which virtually accounts for the entire envelope surface excluding windows, the aggressive and conservative scenarios feature a lower production, equal to about two thirds and one third of the reference scenario, respectively (Fig. 9). Normalized to the heated floor area (HFA), the figures correspond to roughly 40 kW h/m^2 year for the whole envelope (inclusive of windows and unviable surface), 20 kW h/m^2 for the reference scenario, 15 kW h/m^2 year for the aggressive and 10 kW h/m^2 year for the conservative scenario. The inclusion of tree canopies, in this case rendered as completely opaque solid materials (i.e., no solar radiation goes through), implies an obvious and generalized 20 % decrease of energy production in all scenarios. Such more cautious values are assumed for the analyses described further on.

Simulated heating energy needs are represented in Fig. 10a in form of a histogram for the whole district. The average heating needs amount at 138 kW h/m$^2_{HFA}$, with a typical distribution for the Swiss building stock (Cozza et al., 2020). Considering a reversible heat pump system with a yearly average Coefficient of Performance (COP) of 2.8, alternate Current energy production from PV modules is sufficient to cover 32 % of heating energy needs, on average, under a conservative scenario; such share grows to 41 % under an aggressive scenario (Fig. 10b). It is interesting to remark that 40 % of buildings are characterized by a heating coverage factor of less than 20 % (conservative scenario). PV systems that match more than 50 % of heating energy needs are installed in about 30 % of buildings in a conservative scenario. While not addressing here the problem of Urban Heat Island and the impacts of PV modules on outdoor urban climate, it is also interesting to investigate cooling in a future climate-change perspective, considering solar

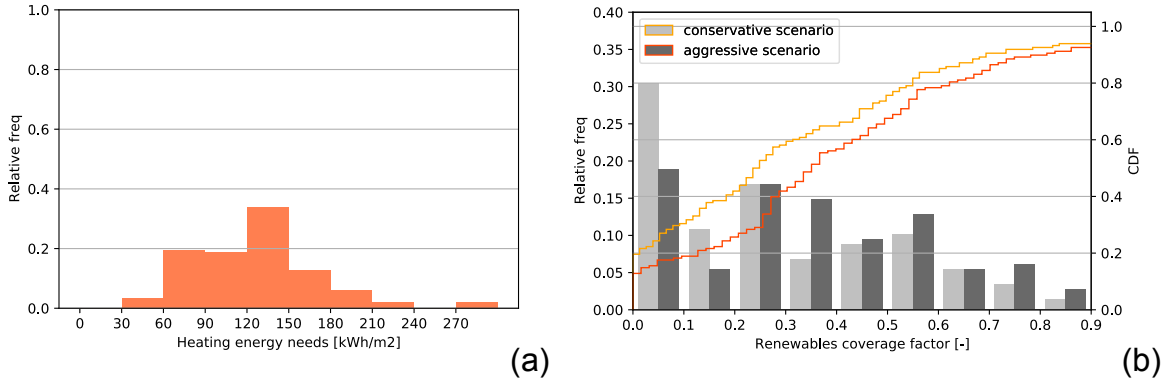

Fig. 10. (a) Distribution of heating energy needs, per bins of 50 kW h/m2 and (b) Heating energy coverage factor from PV modules, calculated as AC current / final energy for heating (Heat-Pump, COP 2.8).

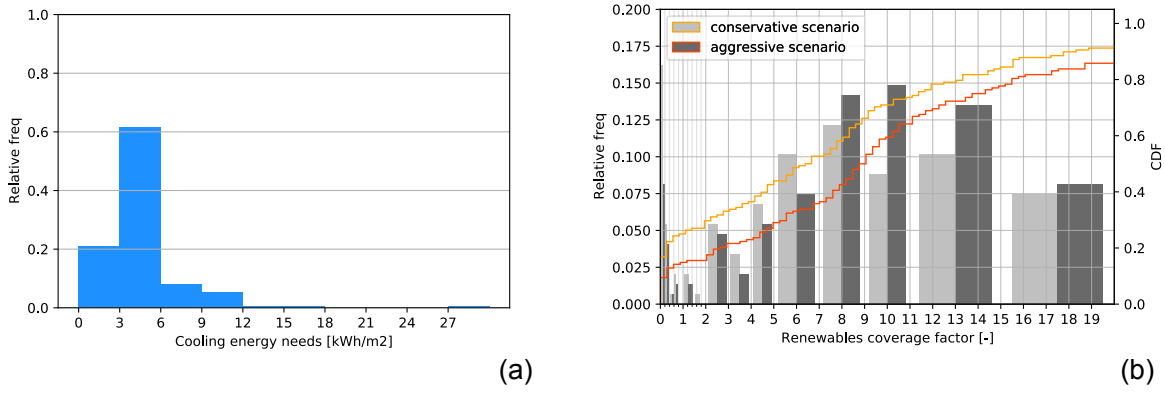

Fig. 11. (a) Distribution of cooling energy needs, per bins of 3 kW h/m2 and (b) Cooling energy coverage factor from PV modules, calculated as AC current / final energy for cooling (Heat-Pump, COP 2.8).

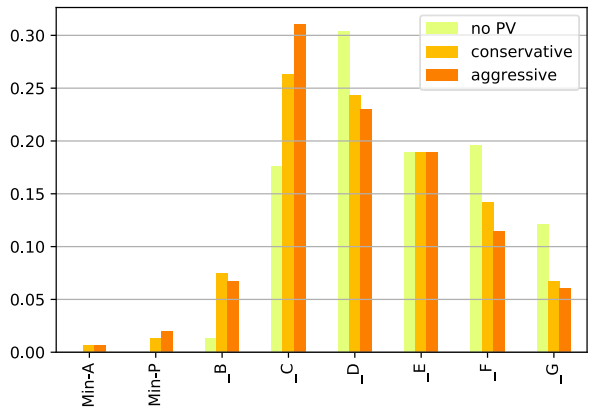

Fig. 12. Energy labels distribution, according to the PV scenarios.

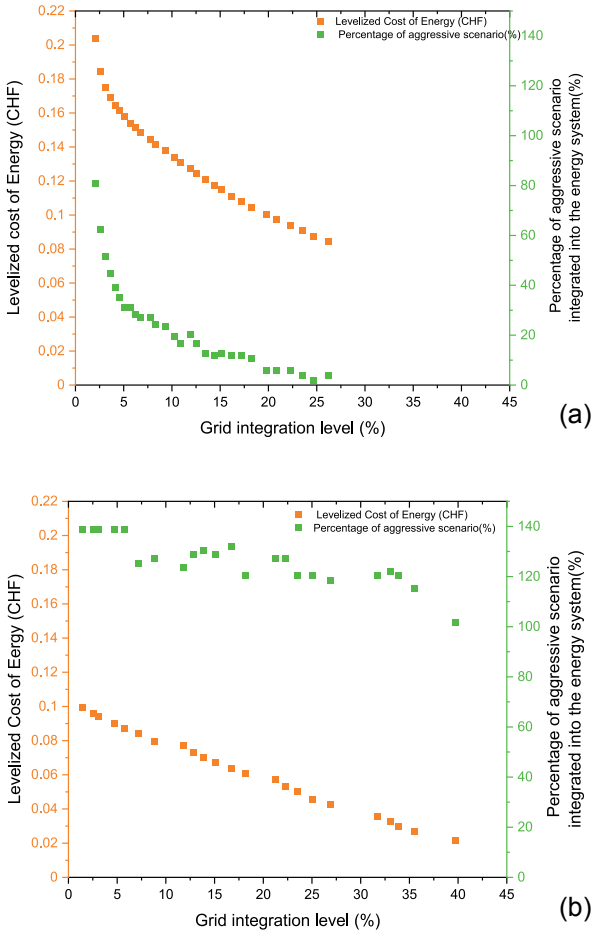

Fig. 13. Levelized cost of energy and potential to integrate PV panels as a percentage of the aggressive scenario taking present (a) and future optimistic (b) scenarios.

electricity as a source for climatization units in form of heat pumps. Almost two thirds of buildings are characterized by cooling needs situated between 3 and 6 kW h/m^2 year (Fig. 11a). For roughly 70 % of the buildings, the cooling needs can be easily covered through PV production, in the majority of cases with an excess electricity to be stored locally or injected to the grid (Fig. 11b).

Considering the all-end-uses energy label (Normalisation Du CECB, 2020), the installation of PV modules allows for a shift between a peak of buildings marked with a "D" label (more than 30 %), to a majority lying in the range above the "C" label under the aggressive scenario (Fig. 12).

The three scenarios present a different renewable energy potential that can be integrated at the building level. However, it is essential to quantify the possibility to incorporate renewable technologies at the system level, considering the limitations such as grid curtailments and energy storage limitations. The Pareto front presented in Fig. 13a shows the alternative designs obtained when simultaneously optimizing the grid integration level and cost considering the system-level limitations. When moving from one Pareto solution to another, either objective function will improve with an inevitable sacrifice in the other objective function.

The solar energy potential notably varies when moving from a conservative scenario to the whole envelope integration scenario. The study reveals that installed PV modules can support a reasonable part of the energy demand by using PV technology (with the support of heat pumps and air conditioning). PV modules can cover a reasonable fraction of the annual energy demand (about 35 %–45 %, depending on the scenario) considering cost optimal operation, which can be increased above 50 % concerning fully autonomous conditions. There is significant PV potential that can be harnessed with the release of grid curtailments, improvements in storage and PV technologies that are worthy to be further investigated.

Several factors hinder the system-level integration. Among these, the higher overall cost for system integration of PV is the main factor that impedes its diffusion. PV generation often does not align with the energy demand, as peak energy demand occurs during the winter nights while the peak generation occurs during summer middays. Whenever there is an excess generation, it needs to be injected into the grid, stored, or curtailed. Lack of grid storage at the local level is a significant problem in this regard. This makes it essential to arrange energy storage, curtail excess generation, or introduce PV installation limitations. However, introducing storage and curtailing the excess generation beyond the grid injection limits makes PV less competitive, leading to a lower installation capacity. However, with the price reduction of PV modules (20 % reduction) and energy storage (20 % reduction), an increase in PV efficiency (20 % increase) and higher limits for grid injection (30 % relaxation of grid curtailments for both injection and purchasing) can make a notable impact (International Energy Agency, 2020). As shown in Fig. 13b, a notable increase in PV capacity can be observed with such an optimistic scenario where grid curtailments are relaxed, PV modules' efficiencies are improved and cost of both energy storage and PV modules are reduced. Finally, it can be stated that the system limits to integrating PV panels are below the visibility limits. Therefore, system integration of PV panels could be performed by maintaining visual acceptability. Although utilizing the full potential of PV generation is not economical concerning the present context, the Pareto front obtained for a future optimistic scenario clearly suggests that PV integration levels can easily pass beyond the visual limits. A joint consideration of visual impact and system integration levels is vital, considering the support offered to urban planners in understanding their mutual influence. Visual impact may be valued of minor importance, since several integration solutions are available on the market of solar modules: however, visibility and quality of solar modules are not the same aspect, they are two distinct and independent variables (Munari Probst & Roecker, 2012). This work focuses on visual impact, while of course high-quality BIPV can also improve the acceptability of highly visible installations.

4. Discussion

Simulated heating energy needs were compared with official data sources to check their validity. Fig. 14a shows the adherence of the simulation with the officially surveyed energy certificates issued by SITG (*SITG - Le Territoire Genevois à La Carte*, 2020). In Fig. 14b, the distribution of heating energy needs per energy construction period is shown, featuring a sound correspondence with a recent publication that regards the whole Swiss territory (Cozza et al., 2020, Fig. 7) (Fig. 14b).

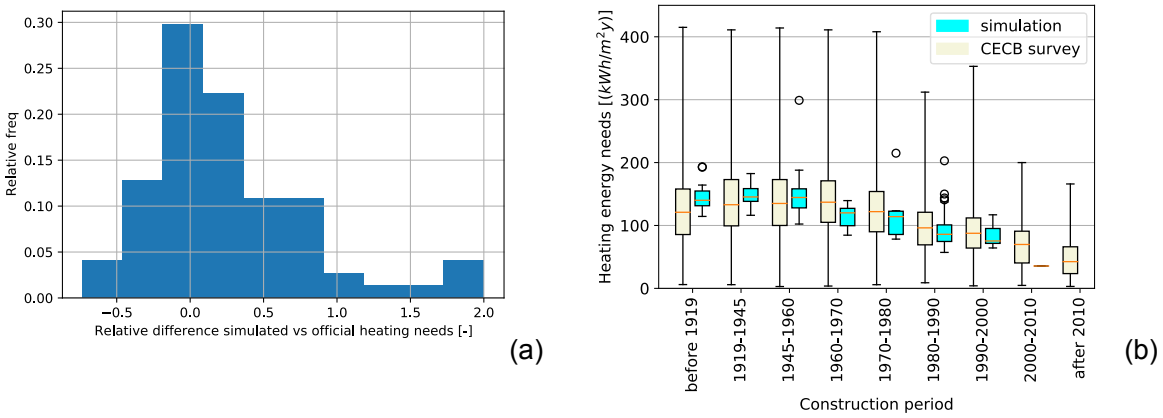

Fig. 14. Relative difference between simulated and officially surveyed buildings (a). Normalized heating energy needs per construction period from the simulation vs the official CECB data (issued from (Cozza et al., 2020)) (b).

Regarding PV production, the employed model is a LOD2+, which includes roof shapes and superstructures: the 3D vector was generated by the cartographic services from a LiDAR point cloud (airborne laser scanner data). Computation time required to simulate highly detailed energy needs of multi-faceted buildings is an issue as it led to a time investment in the adaptation and simplification of the geometry. Despite these limitations, the level of detail of 3D models of cities would likely increase along with computational power: as such, the methodology described hereby will benefit from higher reliability and applicability potential. The main advantages of using such approach relies on the hourly resolution of data, which allows an in-depth analysis, association to 3D city models in the data structure and integration with BIM workflows.

Furthermore, it is worth to discuss the PV match of building energy needs: the heating energy needs are partially covered, while cooling needs, which are in the order of 30 times lower, are totally covered on an annual basis and even exceeded in most cases. Given the correspondence of seasonal PV production peaks with the cooling needs and assuming a growth of cooling needs due to climate change at Swiss latitudes, BIPV should be considered as a suitable strategy for the summer season in a continental climate. Further analysis of the energy demand with the consideration of future climate variations and extreme climate events will help in this regard. At present, 35–45 % of the modules within visibility limits can be incorporated into the energy system concerning low-cost scenarios. The roles of long-term storage and vehicle to grid scenarios are not considered in this study, which will notably increase the solar PV installation capacities. Furthermore, it would be interesting to assess the techno-economic impact on grid reinforcement and grid storage to improve the PV installation limits. Involvement of local and regional planning bodies would play an important role on these regards. Uncertainties brought by the consideration of these potential scenarios in the future would be an interesting direction to look at for further investigation. Overall, there seems to be an appreciable shift in the label of most buildings' primary energy consumption: however, it might be lower than expected, and is insufficient to meet the Minergie® (a Swiss energy-efficiency label) requirements, which should be the target for all buildings undertaking a significant investment to implement building-integrated PV modules. The results of the present study depend on the characteristics of the district, building stock and the climate conditions. Nonetheless, the workflow introduced in the present study can be used globally irrespective of the geographical location, characteristics of the district or building in order to evaluate the feasibility of large-scale PV integration projects.

5. Conclusion

The dissemination of photovoltaic modules integrated in building envelopes requires diffuse and precise information regarding the available solar potential. In this research work, a 3D vector-based model to simulate and assess building energy needs vs BIPV potential at the city scale is presented, together with an economic estimation of PV integration into the grid. An hourly resolution simulation for building energy generation and consumption is carried out with Daysim and CitySim respectively, on typical weather data. The model could be applied to LOD2 city models at the urban scale, considering the potential issued from building envelopes inclusive of façades, shading from vegetation and detailed roof shapes with super-structures. The social acceptability of BIPV is investigated under the aspect of system visibility from the public space, as a significant criterion in the selection of available envelope surface: two scenarios featuring the inclusion of surfaces with different degrees of visibility are discussed. The analysis conducted on a case study indicated that, under an aggressive scenario, a median of 15 kW h_{AC}/m^2_{HFA} year would be available from BIPV production. This amount would be enough to shift the energy label of most buildings by one or two classes, but even with a high autonomy from the grid guaranteed by local storage hubs, only 50 % of generated electricity would likely be used.

It is interesting to remark that, under current operating conditions, a conservative scenario would provide a better grid integration than the aggressive scenario, where most of the energy would be curtailed. In this sense, this paper showed that integrating visibility criteria would not harm the solar energy potential, but rather contribute to size the energy systems to a level that is acceptable for the grid. On the other hand, in a future scenario with an increased grid capacity to accommodate solar electricity, visibility is expected to become a crucial criterion to limit the extent of active PV surface on building envelopes, especially in sensitive contexts, given the released grid integration constraints. BIPV may have a central role in the future decades, with the price reduction of PV modules and energy storage, an increase in PV efficiency and in cooling needs due to climate change: in the cooling season in particular, it constitutes an ideal match between electricity generation and consumption.

Declaration of Competing Interest

The authors report no declarations of interest.

Acknowledgements

This research project was financially supported by the Swiss Competence Center for Energy Research 'Future Energy Efficient Buildings and Districts' (SCCER FEEB&D). Additional funding was provided by the European Union's Horizon 2020 research and innovation program under grant agreement No. 884161. Special

acknowledgements are addressed to the members of the IEA Task 63 Solar Energy Neighborhoods for the inspirational discussions. The code developed in the framework of this project can be found on a Github repository (Florio & Peronato, 2020). PF and GP acknowledge the scientific advice and guidance received during related research work conducted respectively at EPFL LESO-PB and EPFL LIPID.

References

Azzopardi, B., Martínez-Ceseña, E. A., & Mutale, J. (2013). Decision support system for ranking photovoltaic technologies. *IET Renewable Power Generation, 7*(6), 669–679. https://doi.org/10.1049/iet-rpg.2012.0174

Biljecki, F., Stoter, J., Ledoux, H., Zlatanova, S., & Çöltekin, A. (2015). Applications of 3D city models: State of the art review. *ISPRS International Journal of Geo-Information, 4*(4), 2842–2889. https://doi.org/10.3390/ijgi4042842

Bischke, B., Helber, P., König, F., Borth, D., & Dengel, A. (2018). Overcoming missing and incomplete modalities with generative adversarial networks for building footprint segmentation. *ArXiv*, 1808.03195 [Cs] http://arxiv.org/abs/1808.03195.

Building Height 2012—Copernicus Land Monitoring Service. (2020). [Land item]. https://land.copernicus.eu/local/urban-atlas/building-height-2012.

Cassatella, C. (2014). *Linee guida per l'analisi, la tutela e la valorizzazione degli aspetti scenico-percettivi del paesaggio*. Politecnico di Torino.

Catita, C., Redweik, P., Pereira, J., & Brito, M. C. (2014). Extending solar potential analysis in buildings to vertical facades. *Computers & Geosciences, 66*, 1–12. https://doi.org/10.1016/j.cageo.2014.01.002

Costanzo, V., Yao, R., Essah, E., Shao, L., Shahrestani, M., Oliveira, A. C., Araz, M., Hepbasli, A., & Biyik, E. (2018). A method of strategic evaluation of energy performance of Building Integrated Photovoltaic in the urban context. *Journal of Cleaner Production, 184*, 82–91. https://doi.org/10.1016/j.jclepro.2018.02.139

Cozza, S., Chambers, J., & Patel, M. K. (2020). Measuring the thermal energy performance gap of labelled residential buildings in Switzerland. *Energy Policy, 137*, Article 111085. https://doi.org/10.1016/j.enpol.2019.111085

De Medici, S. (2021). Italian architectural heritage and photovoltaic systems. Matching style with sustainability. *Sustainability, 13*(4), 2108. https://doi.org/10.3390/su13042108

Dobos, A. P. (2012). An improved coefficient calculator for the California energy commission 6 parameter photovoltaic module model. *Journal of Solar Energy Engineering, 134*(2). https://doi.org/10.1115/1.4005759

EU-DEM v1.1—Copernicus Land Monitoring Service. (2020). [Land item]. https://land.copernicus.eu/imagery-in-situ/eu-dem/eu-dem-v1.1.

European Commission. (2020a). *Clean energy for all Europeans package*. https://ec.europa.eu/energy/topics/energy-strategy/clean-energy-all-europeans_en.

European Commission. (2020b). *A Renovation Wave for Europe -greening our buildings, creating jobs, improving lives*. https://ec.europa.eu/energy/sites/ener/files/eu_renovation_wave_strategy.pdf.

Florio, P. (2018). *Towards a GIS-Based multiscale visibility assessment method for solar urban planning* (p. 8862). EPFL Thesis n. https://doi.org/10.5075/epfl-thesis-8826.

Florio, P. (2019). *Vertragus/solidangle [Jupyter Notebook]* (Original work published 2019) https://github.com/vertragus/solidangle.

Florio, P., Munari Probst, M. C., Schüler, A., Roecker, C., & Scartezzini, J.-L. (2018). Assessing visibility in multi-scale urban planning: A contribution to a method enhancing social acceptability of solar energy in cities. *Solar Energy, 173*, 97–109. https://doi.org/10.1016/j.solener.2018.07.059

Florio, P., Munari Probst, M. C., Schüler, A., & Scartezzini, J.-L. (2017). Visual prominence vs architectural sensitivity of solar applications in existing urban areas: An experience with web-shared photos. *Energy Procedia, CISBAT 2017 International ConferenceFuture Buildings & Districts – Energy Efficiency from Nano to Urban Scale, 122*, 955–960. https://doi.org/10.1016/j.egypro.2017.07.437

Florio, P., Roecker, C., Munari Probst, M. C., & Scartezzini, J.-L. (2016). Visibility of building exposed surfaces for the potential application of solar panels: A photometric model. *Eurographics Workshop on Urban Data Modelling and Visualisation, a cura di Filip Biljecki e V. Tourre. Liège*. https://doi.org/10.2312/udmv.20161419

Florio, P., & Peronato, G. (2020). *SolViz [Jupyter Notebook]*. https://github.com/vertragus/SolViz.

Freitas, S., Reinhart, C., & Brito, M. C. (2018). Minimizing storage needs for large scale photovoltaics in the urban environment. *Solar Energy, 159*, 375–389. https://doi.org/10.1016/j.solener.2017.11.011

Freitas, S., Serra, F., & Brito, M. C. (2015). Pv layout optimization: String tiling using a multi-objective genetic algorithm. *Solar Energy, 118*, 562–574. https://doi.org/10.1016/j.solener.2015.06.018

Geidl, M., Koeppel, G., Favre-Perrod, P., Klockl, B., Andersson, G., & Frohlich, K. (2007). Energy hubs for the future. *IEEE Power and Energy Magazine, 5*(1), 24–30. https://doi.org/10.1109/MPAE.2007.264850

Grasshopper 3D, algorithmic modeling for Rhino. (n.d.). Retrieved April 5, 2016, from http://www.grasshopper3d.com/.

Groppi, D., de Santoli, L., Cumo, F., & Astiaso Garcia, D. (2018). A GIS-based model to assess buildings energy consumption and usable solar energy potential in urban areas. *Sustainable Cities and Society, 40*, 546–558. https://doi.org/10.1016/j.scs.2018.05.005

Haldi, F., & Robinson, D. (2011). The impact of occupants' behaviour on building energy demand. *Journal of Building Performance Simulation, 4*(4), 323–338. https://doi.org/10.1080/19401493.2011.558213

International Energy Agency. (2020). *World energy outlook 2020 – Analysis*. IEA. https://www.iea.org/reports/world-energy-outlook-2020.

International Energy Agency IEA. (2014). *Technology roadmap: Solar photovoltaic energy*. p. 60. International Energy Agency IEA.

IRENA. (2019). *Solar simulators: Application to developing cities*. IRENA. publications/2019/Jan/Solar-simulators-Application-to-developing-cities.

Jäger-Waldau, A., European Commission, & Joint Research Centre. (2019). *Pv status report 2019*. https://op.europa.eu/publication/manifestation_identifier/PUB_KJNA29938ENN.

Jakubiec, J. A., & Reinhart, C. F. (2013). A method for predicting city-wide electricity gains from photovoltaic panels based on LiDAR and GIS data combined with hourly Daysim simulations. *Solar Energy, 93*, 127–143. https://doi.org/10.1016/j.solener.2013.03.022

Kämpf, J. H., & Robinson, D. (2007). A simplified thermal model to support analysis of urban resource flows. *Energy and Buildings, 39*(4), 445–453. https://doi.org/10.1016/j.enbuild.2006.09.002

Kanters, J., Wall, M., & Kjellsson, E. (2014). The solar map as a knowledge base for solar energy use. *Energy Procedia, 48*, 1597–1606. https://doi.org/10.1016/j.egypro.2014.02.180

Kosorić, V., Lau, S.-K., Tablada, A., & Lau, S. S.-Y. (2018). General model of Photovoltaic (PV) integration into existing public high-rise residential buildings in Singapore – Challenges and benefits. *Renewable and Sustainable Energy Reviews, 91*, 70–89. https://doi.org/10.1016/j.rser.2018.03.087

Ledoux, H., Biljecki, F., Dukai, B., Kumar, K., Peters, R., Stoter, J., & Commandeur, T. (2021). 3dfier: Automatic reconstruction of 3D city models. *Journal of Open Source Software, 6*(57), 2866. https://doi.org/10.21105/joss.02866

Lee, M., Hong, T., Jeong, J., & Jeong, K. (2018). Development of a rooftop solar photovoltaic rating system considering the technical and economic suitability criteria at the building level. *Energy, 160*, 213–224. https://doi.org/10.1016/j.energy.2018.07.020

Lingfors, D., Johansson, T., Widén, J., & Broström, T. (2019). Target-based visibility assessment on building envelopes: Applications to pv and cultural-heritage values. *Energy and Buildings, 204*, Article 109483. https://doi.org/10.1016/j.enbuild.2019.109483

Lobaccaro, G., Lisowska, M. M., Saretta, E., Bonomo, P., & Frontini, F. (2019). A methodological analysis approach to assess solar energy potential at the neighborhood scale. *Energies, 12*(18), 3554. https://doi.org/10.3390/en12183554

Lucchi, E., Garegnani, G., Maturi, L., & Moser, D. (2014). Architectural integration of photovoltaic systems in historic districts. The case study of Santiago de Compostela. *International Conference in Energy Efficiency in Historic Buildings*, 29, 30th https://www.wopapa.it/en/research/institutes/renewableenergy/Publications2/Documents/PaperLucchi-Gar.-Mat.pdf.

Lukač, N., Žlaus, D., Seme, S., Žalik, B., & Štumberger, G. (2013). Rating of roofs' surfaces regarding their solar potential and suitability for PV systems, based on LiDAR data. *Applied Energy, 102*, 803–812. https://doi.org/10.1016/j.apenergy.2012.08.042

Mansouri Kouhestani, F., Byrne, J., Johnson, D., Spencer, L., Hazendonk, P., & Brown, B. (2019). Evaluating solar energy technical and economic potential on rooftops in an urban setting: The city of Lethbridge, Canada. *International Journal of Energy and Environmental Engineering, 10*(1), 13–32. https://doi.org/10.1007/s40095-018-0289-1

Mohajeri, N., Upadhyay, G., Gudmundsson, A., Assouline, D., Kämpf, J., & Scartezzini, J.-L. (2016). Effects of urban compactness on solar energy potential. *Renewable Energy, 93*, 469–482. https://doi.org/10.1016/j.renene.2016.02.053

Munari Probst, M. C., & Roecker, C. (2019). Criteria and policies to master the visual impact of solar systems in urban environments: The LESO-QSV method. *Solar Energy, 184*(May), 672–687. https://doi.org/10.1016/j.solener.2019.03.031

Solar energy systems in architecture (DA 2). In Munari Probst, M. C., & Roecker, C. (Eds.), *IEA SHC Task 41*, (2012).

Normalisation du CECB, Version CECB V5.1.1 (2020). https://www.endk.ch/fr/ablage_fr/politique-energetique/20200402_Normierung_GEAK_EnDK_F.pdf.

Osseweijer, F. J. W., van den Hurk, L. B. P., Teunissen, E. J. H. M., & van Sark, W. G. J. H. M. (2018). A comparative review of building integrated photovoltaics ecosystems in selected European countries. *Renewable and Sustainable Energy Reviews, 90*, 1027–1040. https://doi.org/10.1016/j.rser.2018.03.001

Perera, A. T. D., Wickramasinghe, P. U., Nik, V. M., & Scartezzini, J.-L. (2020). Introducing reinforcement learning to the energy system design process. *Applied Energy, 262*, Article 114580. https://doi.org/10.1016/j.apenergy.2020.114580

Perera, A. T. D., Nik, V. M., Mauree, D., & Scartezzini, J.-L. (2017a). Electrical hubs: An effective way to integrate non-dispatchable renewable energy sources with minimum impact to the grid. *Applied Energy, 190*, 232–248. https://doi.org/10.1016/j.apenergy.2016.12.127

Perera, A. T. D., Nik, V. M., Mauree, D., & Scartezzini, J.-L. (2017b). Electrical hubs: An effective way to integrate non-dispatchable renewable energy sources with minimum impact to the grid. *Applied Energy, 190*, 232–248. https://doi.org/10.1016/j.apenergy.2016.12.127

Perera, A. T. D., Nik, V. M., Mauree, D., & Scartezzini, J.-L. (2017c). An integrated approach to design site specific distributed electrical hubs combining optimization, multi-criterion assessment and decision making. *Energy, 134*, 103–120. https://doi.org/10.1016/j.energy.2017.06.002

Perez, D. (2014). *A framework to model and simulate the disaggregated energy flows supplying buildings in urban areas*, 6112.

Peronato. (2018). *TreeD [C++]*. https://github.com/gperonato/TreeD.

Peronato, G. (2019). *Urban planning support based on the photovoltaic potential of buildings: A multi-scenario ranking system (THESIS)*. Infoscience; EPFL. https://doi.org/10.5075/epfl-thesis-9051

Peronato, Rey, E., & Andersen, M. (2015). Sampling of building surfaces towards an early assessment of BIPV potential in urban contexts. Infoscience *Article CONF. 31st International PLEA Conference* https://infoscience.epfl.ch/record/209966.

Peronato, Rey, E., & Andersen, M. (2016). 3D-modeling of vegetation from LiDAR point clouds and assessment of its impact on façade solar irradiation. *ISPRS - International Archives of the Photogrammetry, Remote Sensing and Spatial Information Sciences*, 67–70. https://doi.org/10.5194/isprs-archives-XLII-2-W2-67-2016. XLII-2/W2.

Peronato, Rastogi, P., Rey, E., & Andersen, M. (2018). A toolkit for multi-scale mapping of the solar energy-generation potential of buildings in urban environments under uncertainty. *Solar Energy, 173*, 861–874. https://doi.org/10.1016/j.solener.2018.08.017

Peronato, G., Rey, E., & Andersen, M. (2018). 3D model discretization in assessing urban solar potential: The effect of grid spacing on predicted solar irradiation. *Solar Energy, 176*, 334–349. https://doi.org/10.1016/j.solener.2018.10.011

QGIS Development Team. (n.d.). QGIS (A Coruña) [C++, Python]. https://www.qgis.org/it/site/.

Reinhart, C. F., & Herkel, S. (2000). The simulation of annual daylight illuminance distributions—A state-of-the-art comparison of six RADIANCE-based methods. *Energy and Buildings, 32*(2), 167–187. https://doi.org/10.1016/S0378-7788(00)00042-6

Rezakhanlou, K., & Frei, E. (2011). *Etude d'integration des panneaux solaires dans la zone ville et villages / Commune de Lutry*. Commune de Lutry.

Robert McNeel & Associates. (n.d.). Rhinoceros 3D (6.0) [Computer software]. www.rhino3d.com.

Robinson, D., & Stone, A. (2004). Solar radiation modelling in the urban context. *Solar Energy, 77*(3), 295–309. https://doi.org/10.1016/j.solener.2004.05.010

Robinson, D., & Stone, A. (2006). Internal illumination prediction based on a simplified radiosity algorithm. *Solar Energy, 80*(3), 260–267. https://doi.org/10.1016/j.solener.2005.02.016

Robinson, D., Haldi, F., Kämpf, J. H., & Perez, D. (2011). Computer modelling for sustainable urban design: Physical principles, methods and applications. *Computer modelling for sustainable urban design*. Earthscan. https://infoscience.epfl.ch/record/165291.

Saretta, E. (2020). A calculation method for the BIPV potential of Swiss façades at LOD2.5 in urban areas_ A case from Ticino region. *Solar Energy, 16*.

Shang, H., & Bishop, I. D. (2000). Visual thresholds for detection, recognition and visual impact in landscape settings. *Journal of Environmental Psychology, 20*(2), 125–140. https://doi.org/10.1006/jevp.1999.0153

Siraganyan, K., Perera, A. T. D., Scartezzini, J.-L., & Mauree, D. (2019). Eco-sim: A parametric tool to evaluate the environmental and economic feasibility of decentralized energy systems. *Energies, 12*(5), 776. https://doi.org/10.3390/en12050776

SITG - Le territoire genevois à la carte. (2020). https://www.etat.ge.ch/geoportail/pro/.

Swiss Federal Council. (2019). *Federal Council aims for a climate-neutral Switzerland by 2050*. August 28 https://www.admin.ch/gov/en/start/documentation/media-releases.msg-id-76206.html.

Swiss Federal Office of Energy. (2019). *Strategie du Programme SuisseEnergie 2021 à 2030*.

Thebault, M., Clivillé, V., Berrah, L., & Desthieux, G. (2020). Multicriteria roof sorting for the integration of photovoltaic systems in urban environments. *Sustainable Cities and Society, 60*, Article 102259. https://doi.org/10.1016/j.scs.2020.102259

Trovato, M. R., Nocera, F., & Giuffrida, S. (2020). Life-cycle assessment and monetary measurements for the carbon footprint reduction of public buildings. *Sustainability, 12*(8), 3460. https://doi.org/10.3390/su12083460

Van der Ham, R., & Idding, J. (1971). In Landbouwuniversiteit Wageningen (Ed.), *De landschapstypologie naar visuele kenmerken. Methoden en gebruik*.

Van Oosterom, A., & Strackee, J. (1983). The solid angle of a plane triangle. *IEEE Transactions on Biomedical Engineering, BME-30*(2), 125–126. https://doi.org/10.1109/TBME.1983.325207

Walch, A., Castello, R., Mohajeri, N., & Scartezzini, J.-L. (2020). Big data mining for the estimation of hourly rooftop photovoltaic potential and its uncertainty. *Applied Energy, 262*, Article 114404. https://doi.org/10.1016/j.apenergy.2019.114404

Walter, E., & Kämpf, J. H. (2015). A verification of CitySim results using the BESTEST and monitored consumption values. *Proceedings of the 2nd Building Simulation Applications Conference*, 215–222.

Wang, Z., & Perera, A. T. D. (2020). Integrated platform to design robust energy internet. *Applied Energy, 269*, Article 114942. https://doi.org/10.1016/j.apenergy.2020.114942